# Reactions of HCl and D2O with Molten Alkali Carbonates

**ARTICLE** *in* THE JOURNAL OF PHYSICAL CHEMISTRY A · FEBRUARY 2011

Impact Factor: 2.69 · DOI: 10.1021/jp107182d · Source: PubMed



**2 AUTHORS**, INCLUDING:

Thomas Krebs
FMC Technologies Inc.
**21** PUBLICATIONS **165** CITATIONS

SEE PROFILE

# Reactions of HCl and $D_2O$ with Molten Alkali Carbonates

**Thomas Krebs and Gilbert M. Nathanson***

*University of Wisconsin-Madison, 1101 University Avenue, Madison, Wisconsin 53706, United States*

*Received: August 10, 2010; Revised Manuscript Received: December 1, 2010*

The acidic oxide $SO_2$ and protic acid HCl are among the gases released in the combustion of coal and the incineration of municipal waste. They are typically removed by wet or dry scrubbing involving calcium carbonate or calcium hydroxide. The molten alkali carbonate eutectic provides a liquid-state alternative that readily absorbs $SO_2$ and HCl and does not become covered with a passivating layer. Gas−liquid scattering experiments utilizing the eutectic mixture (44 mol % $Li_2CO_3$, 31 mol % $Na_2CO_3$, 25 mol % $K_2CO_3$) reveal that the reaction probability for $HCl(g) + CO_3^{2-} \rightarrow CO_2(g) + OH^- + Cl^-$ is 0.31 ± 0.02 at 683 K and rises to 0.39 at 783 K. Gaseous $CO_2$ is formed within $10^{-4}$ s or less, implying that the reaction takes place in a liquid depth of less than 1000 Å. When the melt is exposed to $D_2O$, the analogous reaction $D_2O(g) + CO_3^{2-} \rightarrow CO_2(g) + 2OD^-$ occurs too slowly to measure and no water uptake is observed. Together with previous studies of $SO_2(g) + CO_3^{2-} \rightarrow CO_2(g) + SO_3^{2-}$, these results demonstrate that molten carbonates efficiently remove both gaseous HCl and $SO_2$ while reacting at most weakly with water vapor. The experiments further highlight the remarkable ability of hot $CO_3^{2-}$ ions to behave as a base in reactions with protic and Lewis acids.

## Introduction

The removal of gaseous $SO_2$ in coal-burning power plants is routinely performed by reacting the waste gas stream with limestone (principally $CaCO_3$) or hydrated lime (principally $Ca(OH)_2$) dispersed in water or in solid form.[1] In a recent study, we used gas−liquid scattering experiments to investigate reactions of $SO_2$ with a molten eutectic mixture of alkali carbonates.[2] This work was motivated by studies of Oldenkamp et al.[3] and Atwood et al.,[4] who demonstrated the feasibility of using molten carbonates to remove gaseous $SO_2$ via the reaction

$$SO_2(g) + CO_3^{2-} \rightarrow CO_2(g) + SO_3^{2-} \quad (1)$$

Our scattering experiments indicate that ∼70% of the $SO_2$ molecules that strike the surface of the melt at 683−883 K react to form $CO_2$ in less than $10^{-6}$ s, corresponding to rapid $O^{2-}$ transfer from $CO_3^{2-}$ to $SO_2$ in a shallow liquid region less than 100 Å deep.

Chlorine-rich coal also releases gaseous HCl,[5] as does the incineration of municipal waste containing plastics such as polyvinyl chloride.[6,7] Like $SO_2$, HCl is an acidic gas that should react with molten carbonates. This molten salt may therefore provide an alternative to aqueous carbonate and hydroxide solutions and solid sorbents such as $CaCO_3$, CaO, and $Ca(OH)_2$ for HCl removal.[6,8,9] HCl may react with $CO_3^{2-}$ to generate $CO_2$ according to

$$HCl(g) + CO_3^{2-} \rightarrow CO_2(g) + OH^- + Cl^- \quad (2)$$

Previous studies of HCl removal have focused on the use of solid $CaCO_3$, CaO, and $Ca(OH)_2$. Santschi and Rossi measured the initial uptake of HCl to be 13% on $CaCO_3$ covered with $Ca(OH)(HCO_3)$, created by exposure to water, and identified the surface reaction sites to be $OH^-$ and $HCO_3^-$.[10] The reaction between HCl and $CO_3^{2-}$ itself is difficult to isolate because of this surface hydrolysis at lower temperatures and the conversion of $CO_3^{2-}$ to $O^{2-}$ at high temperatures.[8,11] Despite the 13% reaction probability measured by Santschi and Rossi and the expected reactivity of surface $CO_3^{2-}$, $O^{2-}$, $OH^-$, and $HCO_3^-$ ions, studies utilizing continuous HCl exposures on solid $CaCO_3$, CaO, and $Ca(OH)_2$ report reaction times of seconds to hours, with apparent activation energies between 22 and 84 kJ $mol^{-1}$.[11−18] The longer reaction times are attributed to pore blocking and formation of dense calcium chloride overlayers that impede HCl transport to the underlying solids and, at higher temperatures, to sintering and reverse reactions that regenerate HCl.[7,8,11,14,16,18,19] These studies prompted us to ask if carbonates in the liquid state, where the surface is continuously renewed and the reaction products can dissolve, would capture HCl more efficiently.

The thermochemistry of $SO_2$ and HCl decomposition in molten carbonates has not been measured, but values for the solid-state analogs are given in Appendix I. The detailed mechanism for the reaction between HCl and $CO_3^{2-}$ depends on the timing of H−Cl and $[O-CO_2]^{2-}$ bond breaking: we may imagine two limiting cases in which the reaction proceeds by $H^+$ transfer from HCl to $CO_3^{2-}$ or by $O^{2-}$ transfer from $CO_3^{2-}$ to HCl. If HCl protonates an intact $CO_3^{2-}$, then $HCO_3^-$ would be formed as an intermediate in $CO_2$ production:[10]

$$HCl(g) + CO_3^{2-} \rightarrow HCO_3^- + Cl^- \rightarrow CO_2(g) + Cl^- + OH^- \quad (3)$$

A second mechanism is motivated by the facile transfer of $O^{2-}$ from $CO_3^{2-}$ to the Lewis acid $SO_2$ observed in reaction 1 and by the potentially endothermic decomposition of $HCO_3^-$, as calculated in Appendix I.[2,20] In the case of HCl, $CO_3^{2-}$ may attack the protic acid before it ionizes, generating $CO_2$ and a transient $[OHCl]^{2-}$ complex that decomposes into $OH^-$ and $Cl^-$:

* Corresponding author. E-mail: nathanson@chem.wisc.edu.

10.1021/jp107182d 

$$HCl(g) + CO_3^{2-} \rightarrow CO_2 + [OHCl]^{2-} \rightarrow CO_2(g) + OH^- + Cl^- \quad (4)$$

Our experiments do not discriminate between these pathways because we detect the gaseous $CO_2$ product but not the $HCO_3^-$ and $[OHCl]^{2-}$ intermediates. However, measurements below show that $CO_2$ is formed within $10^{-4}$ s of the HCl collision, implying that any $HCO_3^-$ precursor formed by reaction 3 is not stable and must decay within this time.

Figure 1 illustrates the different trajectories for an HCl molecule impinging on the surface of a molten carbonate that can be explored by molecular beam techniques.[2] HCl may inelastically scatter (IS) from the surface in one or a few collisions or fully dissipate its excess kinetic energy and become momentarily trapped at the surface of the melt. At thermal collision energies, nearly all impinging HCl molecules are expected to equilibrate upon collision with the surface. They can then thermally desorb (TD) from the melt without reacting, dissolve in the melt for long times, or react at the surface or in the bulk with a carbonate ion to produce gaseous $CO_2$ and dissolved $OH^-$ and $Cl^-$. The gas−liquid scattering studies below provide a more detailed picture of these events through measurements of the HCl entry probability into the melt, the probability that these HCl molecules are converted into $CO_2$, the bulk-phase residence time of HCl that do not react, and the time for production of gaseous $CO_2$.

**Acid−Base and Surface Properties of Molten Carbonates.** The alkali carbonate mixture composed of 44 mol % $Li_2CO_3$, 31 mol % $Na_2CO_3$, and 25 mol % $K_2CO_3$ has a eutectic temperature of 672 K.[21,22] It is a clear liquid with a viscosity of ~40 cP.[23] The decomposition of the carbonate anion is governed by the reaction $CO_3^{2-} \rightleftharpoons CO_2(g) + O^{2-}$.[24,25] We previously estimated the equilibrium $CO_2$ vapor pressure of the eutectic melt at 683 K to be $\sim 10^{-7}$ Torr and the $O^{2-}$ concentration to be less than $10^{-6}$ M.[2] In analogy with $H^+$ and $OH^-$ in aqueous solutions, dissolved $CO_2$ and $O^{2-}$ are the strongest acid and base that can exist in molten carbonates.[26] Reactions 1−4 are solute−solvent acid−base reactions: $SO_2$ is a Lewis acid in reaction 1, accepting $O^{2-}$ from solvent $CO_3^{2-}$, whereas HCl is a proton donor in reaction 3 and an $O^{2-}$ acceptor in reaction 4.[27] Our studies show that nearly every $SO_2$ or HCl molecule that disappears into the melt generates one $CO_2$ molecule, implying that reactions 1 and 2 go to completion and, therefore, that $SO_2$ and HCl are stronger acids than $CO_2$ in the molten carbonate system.

Water also behaves like an acid in molten carbonates, but the overall reaction $H_2O(soln) + CO_3^{2-} \rightarrow CO_2(soln) + 2OH^-$ is measured to be endothermic by 90 kJ $mol^{-1}$ at 672 K.[26] As in the case of HCl, the reaction of gaseous $H_2O$ may occur via $H^+$ or $O^{2-}$ transfer:

$$H_2O(g) + CO_3^{2-} \rightarrow OH^- + HCO_3^- \rightarrow 2OH + CO_2(g) \quad (5)$$

and

$$H_2O(g) + CO_3^{2-} \rightarrow [H_2O_2]^{2-} + CO_2(g) \rightarrow 2OH^- + CO_2(g) \quad (6)$$

The studies below indicate that neither reaction occurs to a measurable extent.

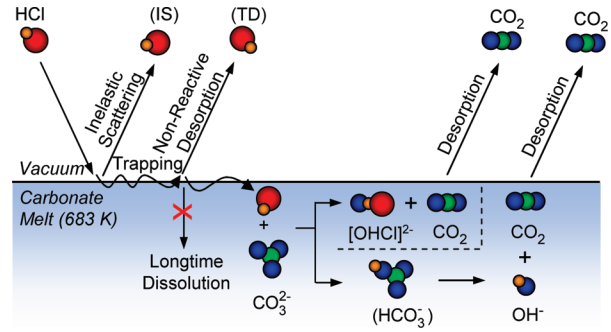


**Figure 1.** Scattering and reaction pathways for an HCl molecule striking the surface of a molten carbonate. The figure illustrates $O^{2-}$ (top, reaction 4) and $H^+$ (bottom, reaction 3) mechanisms for production of $CO_2$.

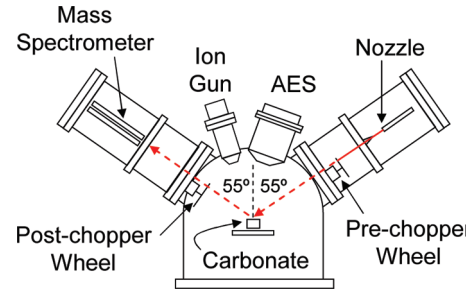


**Figure 2.** Drawing of the experimental apparatus. "AES" denotes Auger electron spectrometer. See text for details.

Little information is available concerning the surface properties of molten alkali carbonates. Kojima and co-workers measured the surface tension of the eutectic mixture to be 230 mN $m^{-1}$ at 672 K, a large value that reflects the ionic nature of the surface region.[28] Their studies also show that the surface tensions of binary and ternary alkali carbonates obey ideal mixing rules, implying that the lower surface tension component preferentially populates the surface layer in the order $K^+ > Na^+ > Li^+$.[29] We do not know the relative populations of the cations and $CO_3^{2-}$ in the outermost layer of the eutectic mixture but note that the top two layers are likely to be composed of both cations and $CO_3^{2-}$ to preserve electrical neutrality.[30]

## Experimental Methods

Figure 2 depicts the scattering apparatus, which has a base pressure of $3 \times 10^{-9}$ Torr and rises to $1 \times 10^{-8}$ Torr with the carbonate present. The experiments are carried out at 683 K (11 K above the eutectic temperature) by directing a collimated and nearly monoenergetic beam of HCl or $D_2O$ molecules at the surface of the molten eutectic and monitoring the reagent gases and the $CO_2$ product, as depicted in Figure 1.

**Preparation and Cleanliness of the Molten Carbonate Eutectic.** $^{13}C$-labeled carbonates were used to circumvent the natural background of $^{12}CO_2$ in the mass spectrometer. $Na_2{}^{13}CO_3$ and $K_2{}^{13}CO_3$ (Sigma-Aldrich, 99%) were used without further purification. $Li_2{}^{13}CO_3$ was not commercially available and $Li_2{}^{12}CO_3$ (Sigma-Aldrich, 98%) was used instead. The eutectic mixture was dried at 423 K for 2 h and then added to a 2 mm deep by 19 mm wide silver crucible, equipped with a 0.81 cm dia button heater.[31] Silver was chosen because of its lack of reactivity with molten salts.[32] When the sample was heated to 683 K for the first time, a gray film appeared on the surface of the otherwise transparent melt. This film is likely composed of insoluble salts and hydrocarbons and was scraped away with a

silver wire. The sample was further sputtered with 2 keV $Ar^+$ ions at a current of 40 mA for 30 min before the start of each experiment.

As described in ref 2, Auger spectra before and after sputtering were recorded at the C, K, and O atom transitions (the Li and Na Auger signals were too weak to measure). The C atom signal decreased and the K and O atom signals increased upon sputtering, most likely from removal of insoluble hydrocarbon impurities. After sputtering, the Auger C:K:O signal ratio remained stable throughout the course of the experiments, and no Ag atom signal originating from the dissolution of the silver crucible was ever observed. This cleanliness and stability were confirmed by high-energy argon atom scattering, which is very sensitive to surface impurities.[2] Additionally, we did not observe a Cl Auger signal from $Cl^-$ accumulation upon HCl exposure at any time during the experiments.

**Molecular Beam Generation.** Each gas mixture is expanded through an 80 $\mu$m diameter nozzle at 450 Torr, which is heated to 383 K to suppress the formation of dimers and clusters, as detailed below. A low-energy HCl beam (7 kJ $mol^{-1}$, $1.3RT_{liq}$) was created by bubbling argon through a 37 wt % aqueous HCl solution at 273 K (~35 Torr HCl vapor pressure). Higher translational energy HCl (94 ± kJ $mol^{-1}$, $17RT_{liq}$) and $D_2O$ (52 kJ $mol^{-1}$, $9RT_{liq}$) beams were created from a 2% HCl in $H_2$ mixture and by bubbling $H_2$ through pure $D_2O$ at 288 K (11 Torr $D_2O$ vapor pressure), respectively. Deuterated water was used to avoid the large $H_2O$ background in the mass spectrometer. In each case, we estimate that the beam fluxes exceed 0.1 monolayers $s^{-1}$.

The monomer to dimer ratio in each mixture was judged by measuring the $HCl^+/H_2Cl^+$ and $D_2O^+/D_3O^+$ ion ratios in the incident beams themselves.[33] We measured ion ratios of $HCl^+/H_2Cl^+ = 100:1$ at 90 kJ $mol^{-1}$ and 40:1 at 11 kJ $mol^{-1}$ and $D_2O^+/D_3O^+ = 30:1$ at 52 kJ $mol^{-1}$. With a sensitivity of 1 part in 400 for HCl and 1 part in 150 for $D_2O$, no signals could be detected at $(HCl)_2H^+$ or $(D_2O)_2D^+$, which are likely to be the dominant ion fragments of $(HCl)_3$ or $(D_2O)_3$, and no signal was detected at $(D_2O)_3D^+$, an ion fragment of $(D_2O)_4$. We also could not detect the parent $(HCl)_2^+$ or $(D_2O)_2^+$ masses. The mixed cluster HClAr was detected at an ion ratio of $HCl^+/(HClAr)^+ \approx 200$. To gauge the effects of the weakly bound $(HCl)_2$ and HClAr species in the 7 kJ $mol^{-1}$ HCl beam, we compare the probabilities for production of $CO_2$ by HCl deposited onto the surface by the 7 and 92 kJ $mol^{-1}$ beams, the latter likely containing very few dimers. We show later that these probabilities are 0.29 ± 0.03 (7 kJ $mol^{-1}$) and 0.27 ± 0.04 (92 kJ $mol^{-1}$). This close agreement suggests that the clusters do not alter the HCl → $CO_2$ reaction probability beyond the 0.02 ± 0.05 difference in the measurements. The $D_2O$ experiments are used primarily to investigate the production of $CO_2$ via reactions 5 and 6. No $CO_2$ was detected upon exposing the melt to the $D_2O$ beam, a result that should not be altered by the presence of water dimers in the $D_2O$ beam.

**Post- and Pre-Chopper Time-of-Flight Spectra.** As depicted in Figure 2, HCl molecules strike a 2.5 × 4.4 $mm^2$ elliptical spot on the carbonate sample at an incident angle $\theta_{inc}$ of 55°. HCl and $CO_2$ molecules exiting in the specular direction are chopped into 70 $\mu$s pulses by a spinning slotted wheel before they are detected by a doubly differentially pumped mass spectrometer. Each of the four slots in the 8.9 cm dia wheel is 0.3 cm wide. The distance between the chopper wheel and the ionizer of the mass spectrometer is $d_{post} = 20.6$ cm. In this postchopper configuration, the arrival time at the mass spectrometer depends only on the velocities of the scattered molecules; these time-of-flight (TOF) spectra are used to determine the energy loss of the impinging molecules and to separate the IS and TD channels illustrated in Figure 1.[34]

Alternatively, the incident beam can be chopped into 70 $\mu$s pulses before it reaches the sample. In this prechopper mode, the flight path is composed of the distance between the sample and the prechopper wheel, $d_{inc} = 13.7$ cm, and the distance between the sample and the ionizer of the mass spectrometer, $d_{pre} = 28.8$ cm. The arrival time at the mass spectrometer is the sum of the gas-phase flight times of the molecule before and after collision with the liquid *and* the residence time of the dissolved reactant and product in solution. As shown previously, this pulsed-beam technique can be used to measure bulk-phase residence times from $10^{-6}$ to $10^{-2}$ s.[35] The pre- and postchopper spectra are displayed on the same postchopper time axis by scaling the prechopper times by $d_{post}/d_{pre}$ and shifting the prechopper spectrum by the flight time of the incident molecules to the sample.

**Uptake Measurements.** The King and Wells[36] method provides a direct means to determine the fraction of impinging molecules that disappear into the melt, either because they react or because they remain dissolved over the duration of the measurement. The uptake probability $p_{uptake}$ is calculated from

$$p_{uptake} = \frac{P_{flag} - P_{liquid}}{P_{flag} - P_{back}} \quad (7)$$

where $P_{flag}$ and $P_{liquid}$ denote the partial pressures of HCl or $D_2O$ in the scattering chamber when the beam is blocked by a Teflon flag from striking the liquid and when it strikes the liquid, respectively. $P_{back}$ denotes the partial background pressure at the reactant mass in the absence of the beam. These partial pressure measurements integrate over all directions of the reflected HCl and $D_2O$ molecules and are not limited to HCl scattering at $\theta_{fin} = 45°$, as monitored in the TOF spectra. The signals were recorded in 600 s intervals at $m/z = 36$ for HCl and $m/z = 20$ for $D_2O$ using the mass spectrometer in Figure 2. When measuring uptake, the postchopper wheel is stationary and blocks the mass spectrometer from directly viewing the sample.

## Results and Analysis

**Low-Energy HCl Uptake.** We first measured the uptake probability $p_{uptake}$ for HCl molecules with an incident energy $E_{inc}$ of 7 kJ $mol^{-1}$. This collision energy is slightly lower than the average flux-weighted translational energy, $2RT_{liq} = 11$ kJ $mol^{-1}$, of molecules striking the surface at $T_{liq} = 683$ K. An average value of $p_{uptake}$ was calculated from 12 individual uptake measurements using eq 7, yielding $p_{uptake} = 0.33 \pm 0.02$ (95% confidence interval). This value implies that one in every three HCl molecules striking the surface of the molten carbonate disappears into solution under near-thermal collision conditions. To determine the fate of these captured HCl molecules as well as those that escape, we next recorded TOF spectra of HCl scattering from the melt and of desorbing $CO_2$ created by gas−liquid reaction.

**Low-Energy HCl Scattering.** Figure 3a shows HCl pre- and postchopper spectra following collisions of HCl molecules with $E_{inc} = 7$ kJ $mol^{-1}$. The postchopper spectrum, which depends only on the velocities of the exiting HCl molecules, is fit well by a Maxwell−Boltzmann (MB) distribution at $T_{liq}$ (solid line). The good MB fit implies that HCl molecules that escape reaction still remain in contact with the melt long enough to thermally

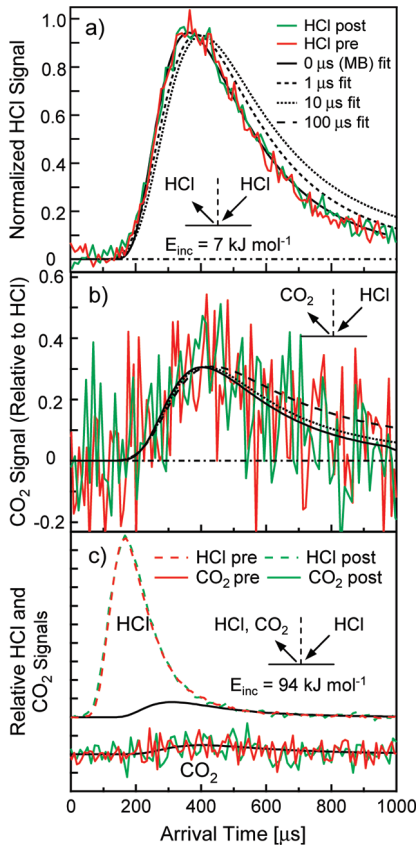


**Figure 3.** (a) Postchopper (green) and prechopper (red) TOF spectra of 7 kJ mol$^{-1}$ HCl molecules scattering from the carbonate melt at 683 K. As described in the text, the calculated TOF spectra correspond to $\tau = 0$ $\mu$s (solid), $\tau = 1$ $\mu$s (short dash), and $\tau = 10$ $\mu$s (dot) bulk-phase residence times. (b) Post- and prechopper spectra for $CO_2$ desorption after HCl → $CO_2$ conversion following collisions of 11 kJ mol$^{-1}$ HCl. The spectra are compared with $\tau = 10$ $\mu$s (dot) and $\tau = 100$ $\mu$s (long dash) calculated curves. (c) Post- and prechopper spectra of 94 kJ mol$^{-1}$ HCl molecules scattering from the carbonate melt and post- and pre- chopper spectra of $CO_2$ desorption. The solid black curves in each panel are Maxwell−Boltzmann distributions at 683 K, for which $\tau = 0$ $\mu$s.

equilibrate before desorbing. These interaction times may range from just a few collisions between HCl and the moving surface alkali and $CO_3^{2-}$ ions, to momentary bonding (trapping) of HCl to these surface species before the HCl desorb, to dissolution deep into the melt before the HCl diffuse back to the surface and desorb.

We can determine if HCl molecules dissolve and reside in solution for longer than $10^{-6}$ s by monitoring the broadening of the prechopper spectrum with respect to the postchopper spectrum. As mentioned above, the arrival times of the HCl molecules in the prechopper spectrum depend on their gas phase flight times and their residence time in the liquid before they desorb, whereas the arrival times in the postchopper spectrum depend only on the velocities of the desorbing HCl. A characteristic residence time for a gas dissolved in solution is defined by the expression for the relative desorption flux, $I_{des}/I_{enter} = 1 - \mathrm{erfc}(\sqrt{t/\tau})\exp(t/\tau)$, obtained by solving the diffusion equation.[34,35] In this expression, $\tau$ is the time in which the outgoing gas flux $I_{des}$ reaches 57% of the flux $I_{enter}$ entering into the liquid as it becomes saturated with gas. The outgoing flux does not reach 95% of the incoming flux until 140 $\tau$ units later (and 99% after 5000 $\tau$ units), because some molecules diffuse deeply into the liquid and do not desorb until much later in time. Thus, even characteristic times as short as $\tau = 10^{-6}$ s lead to a measurable broadening and shifting of the MB distribution to later arrival times using 70 $\mu$s pulses because of the delayed desorption of these deeply diffusing molecules. We have previously used this method to measure the residence times of HCl in supercooled sulfuric acid on the 100 $\mu$s time scale, where the broadening and shifting of the prechopper spectrum are clearly discerned.[37]

Figure 3a shows that the post- and prechopper HCl spectra are identical, with no extra broadening or shift in the prechopper spectrum, indicating that the characteristic residence time for unreactive HCl in the molten carbonate is less than $10^{-6}$ s. Specifically, the $\tau = 1$ $\mu$s (short-dashed line) and 10 $\mu$s (dotted line) desorption profiles generated by 70 $\mu$s pulses are convoluted with an MB distribution to produce the simulated prechopper spectra in Figure 3a. The $\tau = 0$ $\mu$s curve (solid line) is equal to the MB distribution convoluted just with the 70 $\mu$s gas pulse. The $\tau = 1$ and 10 $\mu$s curves are broader than the measured TOF spectra and confirm that the characteristic solvation time is less than $10^{-6}$ s. This upper limit can be used to calculate a maximum characteristic diffusion depth for unreacted HCl into the liquid given by $\langle z(\tau/2)\rangle \approx 0.6(D\tau)^{1/2} \approx 100$ Å using the Stokes−Einstein estimate for $D$ of $1 \times 10^{-6}$ cm$^2$ s$^{-1}$ for a viscosity of 40 cP and a roundtrip transit time of $\tau = 10^{-6}$ s.[38] In the limit in which $\tau \ll 10^{-6}$ s, the unreacted HCl molecules would thermally equilibrate via gas−surface collisions and desorb before penetrating beyond the interfacial region.

The rapid thermalization and desorption channel in Figure 3a accounts for 67% of the incoming HCl flux, based on $p_{uptake} = 0.33$. As shown below, HCl molecules that disappear into the melt produce $CO_2$. We first investigate the time scale for this $CO_2$ production (delay time between HCl entry and $CO_2$ desorption) and then inquire into the possibility of other reaction channels.

**Time Scale for HCl → $CO_2$ Conversion.** Figure 3b shows post- and prechopper $CO_2$ spectra obtained when the sample was exposed to the 7 kJ mol$^{-1}$ HCl beam. The two spectra confirm that $CO_2$ is produced when HCl molecules collide with the carbonate eutectic. As described in Appendix II, these spectra have been corrected for natural $CO_2$ evaporation from the solution. The time required for $CO_2$ production is difficult to determine because the pre- and postchopper spectra are noisy, with no clear evidence that the prechopper spectrum (red) is broadened with respect to the postchopper spectrum (blue). Three simulated fits for $\tau = 0$ s (solid line), 10 $\mu$s (dotted line) and 100 $\mu$s (long-dashed line) are superimposed on the spectra. The simulated 100 $\mu$s fit is significantly broader than the 0 $\mu$s fit; we judge the maximum difference in arrival times between the pre- and postchopper spectra to fall within this broadened region. This comparison implies that the combined characteristic residence times of dissolved HCl, $CO_2$, and any reaction intermediates cannot be greater than 100 $\mu$s, but the noise in the spectra makes it difficult to extract a more precise and potentially much shorter characteristic residence time (which is less than $10^{-6}$ s for $CO_2$ produced from $SO_2$, as shown in ref 2). In particular, the $\tau = 10^{-4}$ s upper limit implies a lifetime for the $HCO_3^-$ intermediate (reaction 3) no longer than this time, which would be created and destroyed within a depth of $0.6(D\tau)^{1/2} < 1000$ Å.

**HCl → $CO_2$ Reaction Probability.** The HCl and $CO_2$ TOF spectra can be combined to determine the fraction of HCl molecules that react to produce $CO_2$. The spectra in Figure 3a,b are first integrated and corrected for the respective ionization cross sections and isotope abundances to obtain the relative

thermal desorption fluxes of detected HCl and $CO_2$ molecules, $I_{HCl}$ and $I_{CO_2}$, as described in Appendix III. The probability $p_{react}$ for conversion of HCl to $CO_2$ can be expressed as the fraction

$$p_{react} = \frac{I_{CO_2}}{I_{HCl} + I_{CO_2}} \quad (8)$$

This expression assumes that HCl and $CO_2$ desorb with the same angular distributions, likely cosine in shape,[39] such that the ratio of fluxes obtained from the TOF spectra at the observation angle of 55° is equal to the ratio of fluxes summed over all exit angles. The TOF spectra in Figure 3a,b yield $p_{react} = 0.29 \pm 0.03$ (95% confidence interval) when averaged over nine independent measurements, yielding a value only slightly smaller than $p_{uptake} = 0.33 \pm 0.02$.

The uptake and reaction probabilities measure different quantities because $p_{uptake}$ is determined by the disappearance of HCl and $p_{react}$ is determined by the appearance of $CO_2$. The two probabilities will differ if some HCl molecules dissolve as neutral or ionic species but do not react to form $CO_2$ (perhaps stopping at $HCO_3^-$), if they react with $O^{2-}$ or $OH^-$ (as outlined in Appendix II) or if $CO_2$ remains dissolved, either molecularly or as $[C_2O_5]^{2-}$.[25] In our case, the similarity between $p_{react}$ and $p_{uptake}$ indicate that almost all HCl molecules that disappear into the melt lead to the production of gaseous $CO_2$. Similar values of $p_{react}$ and $p_{uptake}$ were also found for collisions of $SO_2$ with the molten carbonate.[2] We believe that the best estimate for the HCl → $CO_2$ reaction probability is the average of the two data sets for $p_{react}$ and $p_{uptake}$, equal to 0.31 ± 0.02 (95% confidence interval for 21 measurements).

The short time for HCl → $CO_2$ conversion raises the question of whether HCl molecules can transfer $H^+$ to surface $CO_3^{2-}$ ions in a single collision. This direct reaction would bypass thermal equilibration of HCl and any diffusion into the interfacial region. Evidence against this direct mechanism is given in Figure 3c, which shows identical pre- and postchopper spectra of unreacted HCl and product $CO_2$ following collisions at $E_{inc} = 94$ kJ mol$^{-1}$ ($17RT_{liq}$). At this high energy, only a small fraction of the HCl molecules thermally equilibrate on the surface of the melt. Instead, most HCl recoil directly from the surface, losing on average 60% of their incident energy. The data may be analyzed quantitatively by using the intensities of the HCl and $CO_2$ prechopper spectra to calculate the reaction probability according to eq 8. The relative signals yield $p_{react} = 0.27 \pm 0.04$ (95% confidence interval for seven measurements) when $I_{HCl}$ is set equal to the thermal desorption component of the HCl TOF spectrum, excluding the inelastic scattering component. This value is nearly identical to $p_{react} = 0.29 \pm 0.03$ obtained at a low collision energy of 7 kJ mol$^{-1}$, where almost all HCl molecules thermally equilibrate upon collision. The nearly equal probabilities imply that only thermalized HCl molecules react with $CO_3^{2-}$ to produce $CO_2$ and that a direct gas−surface reaction is unlikely.

**Temperature Dependence of HCl Reactivity.** The HCl → $CO_2$ reaction probabilities $p_{react}$ were measured twice in the cycle 683, 733, and 783 K at $E_{inc} = 7$ kJ mol$^{-1}$. Probabilities obtained from eq 8 are graphed in Figure 4a, together with previously obtained values for $SO_2$ from 683 to 873 K recorded at $E_{inc} = 12$ kJ mol$^{-1}$.[2,40] For HCl, $p_{react}$ increases from 0.31 ± 0.01 at 683 K to 0.39 ± 0.01 at 783 K (error bars are equal to half the difference between the two measurements), while $p_{react}$ remains roughly constant at 0.74 for $SO_2$. The data may be analyzed by equating the ratio of reaction and desorption intensities, $I_{CO_2}/I_{HCl}$, with the ratio of reaction and desorption rate constants. The difference in activation energies for reaction and desorption may then be extracted from the Arrhenius fit shown in Figure 4b. This analysis yields 16 ± 9 kJ mol$^{-1}$ for HCl. A parallel analysis yields −0.3 ± 1.5 kJ mol$^{-1}$ for $SO_2$.

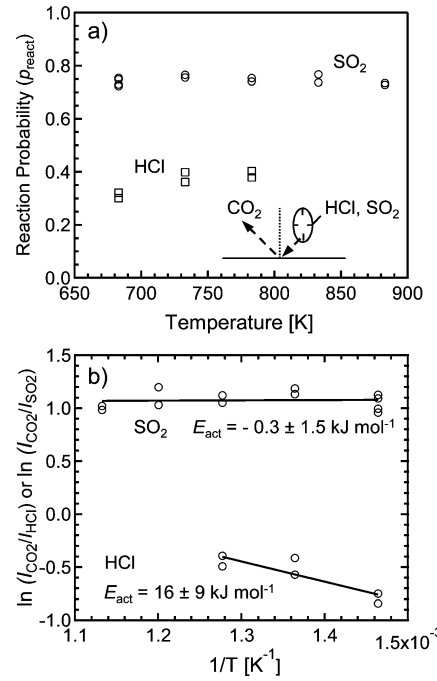


**Figure 4.** (a) HCl reaction probability $p_{react}$ (eq 8) vs temperature $T$ of the carbonate melt. The temperature dependence of the $SO_2$ reaction probability from ref 2 is also shown for comparison. (b) Arrhenius plot of the reaction-to-desorption ratios, $\ln(I_{CO_2}/I_{HCl})$ and $\ln(I_{CO_2}/I_{SO_2})$ vs $1/T$. $E_{act}$ is equal to the difference in activation energies for reaction (HCl → $CO_2$ and $SO_2$ → $CO_2$) and desorption (HCl and $SO_2$).

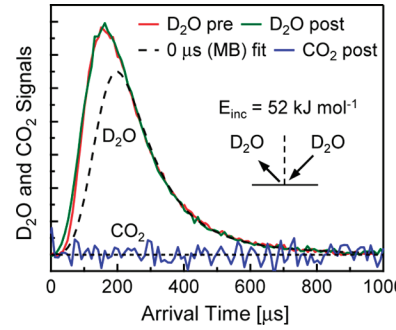


**Figure 5.** Normalized postchopper (green) and prechopper (red) TOF spectra of 52 kJ mol$^{-1}$ $D_2O$ molecules scattering from the carbonate melt at 683 K. The solid black curve is a $D_2O$ Maxwell−Boltzmann distribution at 683 K, for which $\tau = 0$ $\mu$s. The blue line is the $CO_2$ postchopper spectrum that was obtained when the sample was exposed to the $D_2O$ beam.

**Collisions of $D_2O$ with the Carbonate Eutectic.** Figure 5 shows normalized $D_2O$ post- and prechopper spectra following collisions of 52 kJ mol$^{-1}$ ($9RT_{liq}$) $D_2O$ molecules with the alkali carbonate at 683 K. This higher velocity beam was chosen to increase the flux of $D_2O$ molecules striking the surface, while still low enough in energy for many $D_2O$ molecules to thermally equilibrate upon collision. This is confirmed by the substantial overlap of the MB distribution (dashed line) at 683 K with the $D_2O$ postchopper spectrum. $D_2O$ molecules arriving at earlier flight times undergo direct inelastic scattering, losing on average 54% of their energy before recoiling from the surface at $\theta_{fin} =$

55°. The shapes of the post- and prechopper spectra are identical, implying a characteristic bulk-phase residence time shorter than $10^{-6}$ s.

Figure 5 also displays the postchopper spectrum of $CO_2$ that was obtained when the sample was exposed to the $D_2O$ beam. No $CO_2$ signal could be discerned within the statistics of the noise. By comparison with the HCl spectra in Figure 3b, we estimate a $D_2O \rightarrow CO_2$ conversion probability for reaction 4 of less than 1%. The absence of $CO_2$ does not necessarily imply that a reaction does not take place, since $DCO_3^-$ could be formed via reaction 5 but remain in solution as a stable species. To address this question, we measured the net uptake of $D_2O$ into the melt using eq 7 and found $p_{uptake}$ to be $-0.01 \pm 0.02$ (95% confidence interval for six measurements). Together, these measurements indicate that $D_2O$ molecules do not react to produce $CO_2$ or $DCO_3^-$ and do not dissolve for long times in the melt at 683 K.

## Discussion and Conclusions

The scattering experiments reveal that the conversion of HCl to $CO_2$ in the near-surface region of the molten carbonate eutectic proceeds with a steady-state reaction probability of 0.31 $\pm$ 0.02 at 683 K. HCl capture by the melt appears to proceed much more readily than by solid sorbents such as limestone, as summarized in the Introduction. Several possible reasons for the difference between the solid and molten systems include high-temperature sintering and pore blocking and the formation of dense chloride product layers at the surface of solids that impede reaction.[7,8,11,14,16,18,19] In the case of the molten carbonate, the $CO_2$ and HCl mass spectrometer signals did not change over the many hour times of each experiment, equivalent to thousands of monolayers of HCl exposure. We also did not observe any changes in the carbon and oxygen Auger signals over the course of the experiments or detect a chlorine Auger signal. These observations imply that the $Cl^-$ product of reaction 2 does not collect at the surface and impede further reaction, most likely because $Cl^-$ dissolves into the high temperature carbonate melt. The other product of reaction 2, $OH^-$, might react with adsorbed HCl as $OH^-$ accumulates in the melt.[41] It is known to be completely miscible in molten carbonates[42] and is therefore diluted by dissolution. Under our experimental conditions, nearly every HCl molecule absorbed into the melt generates one $CO_2$ molecule, implying that the reaction $HCl + OH^- \rightarrow H_2O + Cl^-$, which does not produce $CO_2$, is superseded by the reaction of HCl with solvent $CO_3^{2-}$ (reaction 2), which releases $CO_2$. Appendix II lists other reactions of HCl that also do not produce $CO_2$.

The high 30−40% reaction probability of HCl with the molten carbonate over 683 to 783 K, in combination with the steady ~70% reactivity of $SO_2$, highlights the remarkable ability of $CO_3^{2-}$ and alkali ions to capture and hold HCl and $SO_2$ long enough to react. As depicted in Figure 1, impinging HCl molecules first become momentarily trapped at the surface upon collision and then react with $CO_3^{2-}$ in the interfacial region or just below it. This two-step trapping and reaction process is supported by the equal reactivities of thermally equilibrated HCl molecules deposited by the 7 and 94 kJ $mol^{-1}$ beams, which suggest that only these thermalized HCl molecules generate $CO_2$. The remaining HCl molecules desorb back into the gas phase; Figure 4 indicates that HCl desorption outpaces $HCl \rightarrow CO_2$ conversion from 683 to 783 K and that $CO_2$ production is not predicted to match HCl desorption until ~930 K. In comparison, the steady ~70% reaction probabilities for $SO_2$ indicate that $CO_2$ production is more likely than desorption. Arrhenius fits to the data in Figure 4b yield differences in the reaction and desorption activation energies of ~16 kJ $mol^{-1}$ ($3RT_{liq}$) for HCl and less than 1 kJ $mol^{-1}$ for $SO_2$, implying that HCl binds more weakly than $SO_2$ to the surface and/or encounters a larger barrier for conversion to $CO_2$.

Reactions 3 and 4 provide two different pathways for generating $CO_2$ from HCl. The molecule may react by protonating $CO_3^{2-}$ near the surface, followed by conversion of $HCO_3^-$ into $CO_2$ and $OH^-$ within $10^{-4}$ s. This initial protonation might be expected for a strong acid such as HCl, which would generate an $HCO_3^-$ intermediate that then decomposes within $10^{-4}$ s (the maximum characteristic time estimated from Figure 3b). As calculated in Appendix I, however, the decomposition of $HCO_3^-$ itself may be very endothermic. Alternatively, HCl may be attacked by $CO_3^{2-}$ via $O^{2-}$ transfer, directly generating $CO_2$ along with a transient $[OHCl]^{2-}$ complex that decays into $Cl^-$ and $OH^-$. In both cases, adequate solvation of the reactants and products likely requires the H atom of HCl to point toward an O atom of $CO_3^{2-}$, while the Cl atom points toward one or more $Na^+$, $Li^+$, or $K^+$ ions in the near-interfacial region. A similar mechanism has been proposed for reactions of $SO_2$ at the surface of solid CaO; in this case, $O^{2-}$ transfer occurs after the S atom of $SO_2$ points toward the O atom of CaO and the O atoms of $SO_2$ each point toward a $Ca^{2+}$ ion.[43,44] Within this picture, the different HCl and $SO_2$ reactivities may arise from differences in ion-HCl and ion-$SO_2$ solvation and the ease with which $CO_3^{2-}$ transfers $O^{2-}$ to each species. This reactivity is suppressed, however, in the case of $D_2O$: Figure 5 shows that nearly all impinging $D_2O$ molecules desorb from melt before they can react, either by $D_2O$ dissociation (reaction 5) or by $O^{2-}$ transfer (reaction 6). This absence of reactivity is in accord with the measured 90 kJ $mol^{-1}$ endothermicity of the reaction $H_2O + CO_3^{2-} \rightarrow CO_2 + 2OH^-$ in the molten carbonate.[26]

The high HCl and $SO_2$ reactivities at temperatures above 672 K shown in Figure 4 may be advantageous from a practical standpoint because they imply that efficient HCl and $SO_2$ removal is not confined to temperatures near the eutectic point, where product chlorides and sulfates (from oxidation of $SO_3^{2-}$) may be less soluble or cause solidification of the melt upon extended exposure.[4] This insensitivity, when combined with the near-interfacial capture of HCl and $SO_2$, suggests that thin flowing films of molten carbonates over a wide temperature range may provide a versatile means to remove HCl and $SO_2$ from waste gases with potentially little interference from ambient water. These high reactivities further suggest that the molten carbonate eutectic may also readily react with other important protic acids and acidic oxides, including $HNO_3$ and $N_2O_5$.[45−47]

**Acknowledgment.** This material is based on work supported by the National Science Foundation under Grant No. CHE-0809681. We are grateful to NSF for funding this work and to the Deutsche Forschungsgemeinschaft for a research fellowship for T.K. under Grant No. KR 2935/2-1. We also thank the reviewers for inquiring about dimer concentrations in the incident beams and L. Dempsey and J. Faust for measuring monomer to dimer ion ratios.

## Appendix I: Thermochemistry of HCl and $SO_2$ Reactions.

The enthalpies and free energies of reations 1−4 are not known in any molten carbonate. The closest analogs for which thermodynamic information is available are perhaps the solid-state conversions at 683 K for the sodium salts (reaction 4 has no analog).[4] The values for NaOH and $NaHCO_3$ have been extrapolated from the solid to 683 K without phase change:[48]

$$SO_2(g) + Na_2CO_3(s) \rightarrow CO_2(g) + Na_2SO_3(s)$$
$$\Delta H^\circ \approx -67 \text{ kJ mol}^{-1} \text{ and } \Delta G^\circ \approx -41 \text{ kJ mol}^{-1} \quad \text{(A.1)}$$

and

$$HCl(g) + Na_2CO_3(s) \rightarrow CO_2(g) + NaOH(s) + NaCl(s)$$
$$\Delta H^\circ \approx -6 \text{ kJ mol}^{-1} \text{ and } \Delta G^\circ \approx -25 \text{ kJ mol}^{-1} \quad \text{(A.2)}$$

The decomposition of HCl can be broken into two steps mimicking reaction 3:

$$HCl(g) + Na_2CO_3(s) \rightarrow NaHCO_3(s) + NaCl(s)$$
$$\Delta H^\circ \approx -130 \text{ kJ mol}^{-1} \text{ and } \Delta G^\circ \approx -29 \text{ kJ mol}^{-1} \quad \text{(A.3a)}$$

and

$$NaHCO_3(s) \rightarrow CO_2(g) + NaOH(s)$$
$$\Delta H^\circ \approx +124 \text{ kJ mol}^{-1} \text{ and } \Delta G^\circ \approx +4 \text{ kJ mol}^{-1} \quad \text{(A.3b)}$$

These reactions may not be adequate analogs, however, because reactions 1−4 represent transformations of HCl and $SO_2$ at infinite dilution in the molten carbonate solvent, whereas reactions A.1−A.3 represent the full conversion of solid-state reactants into solid-state products, accompanied by abrupt changes in system composition. In particular, the formation of $HCO_3^-$ in A.3a is extremely exothermic and its decomposition in A.3b is extremely endothermic. If the $HCO_3^-$ intermediate thermalizes before it decomposes, then this endothermicity must be much smaller in molten carbonates for a bicarbonate precursor to be plausible given the observed overall activation energy of ~16 kJ mol$^{-1}$.

## Appendix II: $CO_2$ Evaporation and Reactions of Gases with Trace $O^{2-}$ and HCl with Itself.

The $CO_2$ post-chopper spectra in Figure 3b,c have been corrected for natural $CO_2$ evaporation from the 683 K sample. This evaporation is caused by the decomposition of $CO_3^{2-}$ into $CO_2$ and $O^{2-}$ according to $K_{eq} = [O^{2-}]P_{CO_2} < 10^{-13}$. At 683 K, the $CO_2$ vapor pressure above a freshly prepared eutectic melt is $\sim 10^{-7}$ mbar.[2] Over the course of several days, this signal decreased and eventually disappeared within the statistics of the background signal as $CO_2$. This disappearance is caused by $CO_2$ evaporation itself, which raises the $O^{2-}$ concentration and suppresses further $CO_2$ production. In all cases, the natural $CO_2$ evaporation did not exceed 10% of the $CO_2$ signal obtained from exposure to HCl. $CO_2$ evaporation is not a concern when recording pre-chopper spectra because it is not correlated with the incident HCl pulse train and instead contributes only to the average $CO_2$ background. For this reason, all calculations of $p_{react}$ according to eq 8 utilize pre-chopper rather than post-chopper spectra.

Trace $O^{2-}$ in the carbonate melt can potentially react with HCl, $SO_2$, and $H_2O$ in the near-surface region according to the reactions $HCl + O^{2-} \rightarrow OH^- + Cl^-$, $SO_2 + O^{2-} \rightarrow SO_3^{2-}$, and $H_2O + O^{2-} \rightarrow 2OH^-$. These reactions do not produce $CO_2$ and are therefore unlikely to contribute substantially because of the good agreement between $p_{react} = 0.29 \pm 0.03$ and $p_{uptake} = 0.33 \pm 0.02$. These values predict a maximum contribution of $0.04 \pm 0.04$ for $HCl + O^{2-}$, or roughly 13% of the total destruction rate. In the case of $SO_2$, we measured $p_{react}$ to be slightly greater than $p_{uptake}$ and therefore found no evidence for the reaction $SO_2 + O^{2-} \rightarrow SO_3^{2-}$. The lack of $CO_2$ production upon exposure to $D_2O$ is also in accord with the measured absence of $D_2O$ uptake. The general lack of reactivity with $O^{2-}$ is likely due to the very low $O^{2-}$ concentrations in our experiments, which must lie between the equilibrium value of $10^{-6}$ M and the maximum $O^{2-}$ solubility of 0.02 M.[49,50]

The good agreement between $p_{react}$ and $p_{uptake}$ also implies that reactions originating from two HCl molecules do not occur significantly. These include reactions of HCl with product $OH^-$ or precursor $HCO_3^-$ or between $HCO_3^-$ species (which are created by HCl via reaction 3):

$$HCl(g) + OH^- \rightarrow H_2O + Cl^-$$

$$HCl(g) + HCO_3^- \rightarrow CO_2(g) + Cl^- + OH^-$$

$$2HCO_3^- \rightarrow CO_2(g) + CO_3^{2-} + H_2O(g)$$

Each of these reactions starts with two HCl and produces one $CO_2$. They should become more likely with increasing concentrations of product $OH^-$ and any precursor $HCO_3^-$.

## Appendix III: Reaction Probabilities from TOF Spectra.

The HCl and $CO_2$ mass spectrometer signals may be converted into relative fluxes in the following way. For a molecule A, the mass spectrometer ion signal $n_{A^+}$ is proportional to the number density $n_A$ through the relation $n_{A^+} = n_A T_{A^+} \sigma_{A^+} f_A$, where $T_{A^+}$ is the transmission efficiency of the mass spectrometer for the ion $A^+$, $\sigma_{A^+}$ is the partial ionization cross section for creation of $A^+$, and $f_A$ denotes the relative isotopic abundance of A. The desorption flux $I_A$ at an exit angle of 55° is then obtained from the pre-chopper TOF spectrum according to $I_A = \int n_A v_A dv_A$, where $v_A$ is the velocity of the gas phase molecule, equal to $d_{post}/t_A$, and $t_A$ is the time of arrival. The angular distributions of desorbing HCl and $CO_2$ are assumed to be the same (and likely cosine), so that the ratio of fluxes at 55° is equal to the ratio of fluxes integrated over all exit angles. These fluxes are in turn proportional to the probabilities for the production of $CO_2$ or scattering of HCl or $SO_2$.

The natural abundances $f$ of the species are 0.758 ($^1H^{35}Cl$) and 0.567 ($^{13}C^{16}O_2$), taking into account the enhanced concentration of $^{13}C$ in the sample. Partial ionization cross sections for the molecules at 100 eV electron impact energy are 3.88 Å$^2$ (HCl) and 2.25 Å$^2$ ($CO_2$).[51,52] We assume that the transmission functions, which depend on mass, are equal for $^{13}CO_2^+$ (45 amu) and $HCl^+$ (36 amu). This approximation yields $n_{CO_2}/n_{HCl} = 2.31 n_{CO_2^+}/n_{HCl^+}$. In our experiments, the thermal desorption distributions are well fit by Maxwell-Boltzmann distributions, and the ratio of fluxes becomes $I_{CO_2}/I_{HCl} = 2.31(\langle v_{CO_2}\rangle / \langle v_{HCl}\rangle)(n_{CO_2^+}/n_{HCl^+}) = 2.06 n_{CO_2^+}/n_{HCl^+}$.

## References and Notes

(1) Srivastava, R. K.; Jozewicz, W. *J. Air Waste Manage. Assoc.* **2001**, *51*, 1676.
(2) Krebs, T.; Nathanson, G. M. *Proc. Natl. Acad. Sci. U.S.A.* **2010**, *107*, 6622.
(3) Oldenkamp, R. D.; Margolin, E. D. *Chem. Eng. Prog.* **1969**, *65*, 73.

(4) McIlroy, R. A.; Atwood, G. A.; Major, C. J. *Environ. Sci. Technol.* **1973**, *7*, 1022.
(5) Ydovich, Y. E.; Ketris, M. P. *Coal Geol.* **2006**, *67*, 127.
(6) Yan, R.; Chin, T.; Liang, D. T.; Laursen, K.; Ong, W. Y.; Yao, K.; Tay, J. H. *Environ. Sci. Technol.* **2003**, *37*, 2556.
(7) Shemwell, B.; Levendis, Y. A.; Simons, G. A. *Chemosphere* **2001**, *42*, 785.
(8) Partanen, J.; Backman, P.; Backman, R.; Hupa, M. *Fuel* **2005**, *84*, 1664.
(9) U.S. Environmental Protection Agency, Flue gas desulfurization (acid removal), yosemite.epa.gov/oaqps/EOGtrain.nsf/DisplayView/SI_412C_9?OpenDocument and _412C_7?OpenDocument.
(10) Santschi, C.; Rossi, M. J. *J. Phys. Chem. A* **2006**, *110*, 6789.
(11) Gullett, B. K.; Jozewicz, W.; Stefanski, L. A. *Ind. Eng. Chem. Res.* **1992**, *31*, 2437.
(12) Daoudi, M.; Walters, J. K. *Chem. Eng. J.* **1991**, *47*, 1.
(13) Mura, G.; Lallai, A. *Chem. Eng. Sci.* **1994**, *49*, 4491.
(14) Duo, W.; Kirkby, N. F.; Seville, J. P. K.; Clift, R. *Chem. Eng. Sci.* **1995**, *50*, 2017.
(15) Wang, W.; Zhicheng, Y.; Bjerle, I. *Fuel* **1996**, *75*, 207.
(16) Fonseca, A. M.; Órfão, J. J.; Salcedo, R. L. *Ind. Eng. Chem. Res.* **1998**, *37*, 4570.
(17) Li, M.; Shaw, H.; Yang, C.-L. *Ind. Eng. Chem. Res.* **2000**, *39*, 1898.
(18) Verdone, N.; De Filippis, P. *Chem. Eng. Sci.* **2006**, *61*, 7487.
(19) Weinell, C. E.; Jensen, P. I.; Dam-Johansen, K.; Livbjerg, H. *Ind. Eng. Chem. Res.* **1992**, *31*, 164.
(20) Thompson, M. M.; Palmer, R. A. *Appl. Spectrosc.* **1988**, *42*, 945.
(21) Janz, G. J.; Lorenz, M. R. *J. Chem. Eng. Data* **1961**, *6*, 321.
(22) Ward, A. T.; Janz, G. J. *Electrochim. Acta* **1965**, *10*, 849.
(23) Ejima, T.; Sato, Y.; Yamamura, T.; Tamal, K.; Hasebe, M.; Bohn, M. S.; Janz, G. J. *J. Chem. Eng. Data* **1987**, *32*, 180.
(24) Baker, E. H. *J. Chem. Soc.* **1962**, 464.
(25) Claes, P.; Moyaux, D.; Peeters, D. *Eur. J. Inorg. Chem.* **1999**, *4*, 583.
(26) Janz, G. J. *J. Chem. Educ.* **1967**, *44*, 581.
(27) Jensen, W. B. *The Lewis Acid-Base Concepts*; Wiley: New York, 1980.
(28) Kojima, T.; Miyazaki, Y.; Nomura, K.; Tanimoto, K. *J. Electrochem. Soc.* **2008**, *155*, F150.
(29) Defay, R.; Prigogine, I. *Surface Tension and Adsorption*; Wiley: New York, 1966; Ch. 7.
(30) The most stable surface of solid $CaCO_3$ is composed equally of calcium and tilted carbonate ions, with O atoms above, below, and in the surface plane. See Figure 1 of Kerisit, S.; Parker, S. C.; Harding, J. H. *J. Phys. Chem. B* **2003**, *107*, 7676–7682.
(31) Heat Wave Labs model #101136.
(32) Wyatt, M.; Fisher, J. M. *Platinum Met. Rev.* **1988**, *32*, 200.
(33) Dyke, T. R.; Muenter, J. S. *J. Chem. Phys.* **1972**, *57*, 5011.
(34) Nathanson, G. M. *Annu. Rev. Phys. Chem.* **2004**, *55*, 231.
(35) Morris, J. R.; Behr, P.; Antman, M. D.; Ringeisen, B. R.; Splan, J.; Nathanson, G. M. *J. Phys. Chem. A* **2000**, *104*, 6738.
(36) King, D. A.; Wells, M. G. *Proc. R. Soc. London, Ser. A* **1974**, *339*, 245.
(37) Lawrence, J. R.; Glass, S. V.; Park, S.-C.; Nathanson, G. M. *J. Phys. Chem. A* **2005**, *109*, 7458.
(38) The diffusion depth is estimated by calculating $\langle z(\tau/2)\rangle = [\int zc(z,\tau/2)/c^* dz]/[\int c(z,\tau/2)/c^* dz] = 0.60(D\tau)^{1/2}$ for a diffusion time of $\tau/2$. This concentration profile is obtained from the diffusion equation, as outlined in ref 35. It is given by $c(z,t)/c^* = \mathrm{erfc}(z/(4Dt)^{1/2}) - \exp(z/(Dt))^{1/2}\exp(t/\tau)\,\mathrm{erfc}((t/\tau)^{1/2} + z/(4Dt)^{1/2})$, where erfc is the complementary error function.
(39) Rettner, C. T.; Schweizer, E. K.; Mullins, C. B. *J. Chem. Phys.* **1989**, *90*, 3800.
(40) The incident $SO_2$ incident energy was mistakenly reported as 16 kJ $mol^{-1}$ in ref 2.
(41) Partanen, J.; Backman, P.; Backman, R.; Hupa, M. *Fuel* **2005**, *84*, 1674.
(42) Reshetnikov, N. A.; Perfil'eva, O. G. *Russ. J. Inorg. Chem.* **1968**, *13*, 1662.
(43) Pacchioni, G.; Ricart, J. M.; Illas, F. *J. Am. Chem. Soc.* **1994**, *116*, 10152.
(44) Rodriguez, J. A.; Jirsak, t.; Freitag, A.; Larese, J. Z.; Maiti, A. *J. Phys. Chem. B* **2000**, *104*, 7439.
(45) Al-Hosney, H. A.; Grassian, V. H. *Phys. Chem. Chem. Phys.* **2005**, *7*, 1266.
(46) Karagulian, F.; Santschi, C.; Rossi, M. J. *Atmos. Chem. Phys.* **2006**, *6*, 1373.
(47) Mogili, P. K.; Kleiber, P. D.; Young, M. A.; Grassian, V. H. *Atmos. Environ.* **2006**, *40*, 7401.
(48) Thermochemical data available at http://webbook.nist.gov/chemistry/ and from *Thermochemical Properties of Inorganic Substances*; Knacke, O., Kubaschewski, O., Hesslemann, K., Eds.; Springer-Verlag: Berlin, 1991.
(49) White, S. H.; Twardoch, U. M. *J. Appl. Electrochem.* **1989**, *19*, 901.
(50) See supplemental information in ref 2 at www.pnas.org/cgi/content/full/0910993107/DCSupplemental.
(51) Ali, M. A.; Kim, Y. K. *J. Phys. B* **2008**, *41*, 145202.
(52) Itikawa, Y. *J. Phys. Chem. Ref. Data* **2002**, *31*, 749.

JP107182D